Applied Surface Science Advances 19 (2024) 100571



Contents lists available at ScienceDirect

Applied Surface Science Advances

journal homepage: www.sciencedirect.com/journal/applied-surface-science-advances





Evaluation of intelligent packaging functions of black carrot extract-infused polyvinyl alcohol nanofibers

Turgay Cetinkaya

Department of Food Processing, Armutlu Vocational School, Yalova University, Armutlu, Yalova 77500, Türkiye

A R T I C L E I N F O

Keywords:
Smart packaging
Black sea salmon
Volatile amine
Gas absorption
Surface structure

A B S T R A C T

In this study, we aimed to evaluate the characteristic changes in polyvinyl alcohol-based nanofibers after being stored with black sea salmon fillets. For this purpose, electrospun nanofibers were produced as control (PVA), black carrot extract-incorporated (PVAB), and extract+SnO_2 incorporated (PVASN), and their properties were compared. Morphological results showed the formation of regular ultrafine nanostructures, and differences between nanofiber samples were evaluated by measuring fiber diameters. Nanofiber sizes increased with the addition of black carrot and SnO_2. Elemental analysis was performed to obtain information about the concentration in the nanofibers. Different O and Sn concentrations indicated that important constituents of anthocyanins and SnO_2 were attached to the samples. The location of C, O, Sn atoms was determined by Energy Spectrum Analysis (EDS) color mapping, which confirmed the attachment of Sn in the PVASN sample. To elucidate the relationship between spoilage and the absorption of volatiles from smoked salmon fillets, nanofibers and fillets were kept together in a petri dish at room temperature. After being stored with salmon meat, the PVASN sample showed fewer entanglements without any defects. Upon exposure to volatiles, molecular structures changed, and water contact angle values decreased. X-Ray Diffraction (XRD) results indicated the state of the polymer matrix and SnO_2. Chemical bond interactions with released volatiles effected the peak parameters of nanofibers. 3D and 2D surface topographical images of PVASN were also compared before and after storage using a profilometer. This study's results showed that functionalized nanofibers with extract-SnO_2 could be applied as an intelligent food packaging layer, providing valuable data about the potential usage of electrohydrodynamic processing.

1. Introduction

It is important for consumers to predict the quality of processed fish products before consumption [1]. Real-time determination of spoilage in fish products is vital for consumers. During fish spoilage, the loss of volatile nitrogen-containing compounds, such as biogenic amines, NH_3, dimethlyamine (DMA), and trimethlyamine (TMA), causes a change in the pH of products. The implementation of intelligent freshness indicators is essential for the detection of quality. Therefore, novel smart packaging materials have been proposed in recent years [2–4]. For instance, black carrots (*Daucus carota sativus* var. *atrorubens*) are native to Türkiye and the Far East and have been grown for thousands of years. They have been successfully used in the food industry as a colorant due to their high heat, light, and pH stability. Moreover, since they are cheap and easily accessible, they can be considered for the development of functionalized nanomaterials with low production costs. Recent studies have been carried out using black carrot extracts as a nanofibrous sensor indicator. The use of a smart pH-sensing indicator based on nanocellulose and black carrot to monitor the freshness of fish fillets during storage has been investigated [2]. Pakolpakçıl et al. [5] blended black carrot extract with polyvinyl alcohol and sodium alginate to develop pH-sensing nanofibrous mats.

In recent years, electroshydrodynamic processing techniques have been utilized as novel approaches to the development of intelligent packaging systems. Electrospinning is a method to produce nanofibers under high voltage. Nanofibers are defined as cylindrical structures that generally have a size of less than 1 μm. Parameters such as applied voltage, distance, and feed rate can affect nanofiber morphology and diameter [6]. When the fiber's diameter reaches the nanometer size, surface area increases. High surface area and porosity lead to nanofiber surface functionalization with nanoparticles. These properties make nanofibers potential candidates for smart packaging applications. Furthermore, the high surface area may enhance the reactivity of the material and may speed up adsorption. Therefore, the possibility to fill this nanomaterial with gas or volatile and biochemical species may open methods [6,7].

E-mail address: turgay.cetinkaya@yalova.edu.tr.

https://doi.org/10.1016/j.apsadv.2023.100571
Received 25 September 2023; Received in revised form 31 December 2023; Accepted 31 December 2023
Available online 5 January 2024
2666-5239/© 2024 The Author(s). Published by Elsevier B.V. This is an open access article under the CC BY license (http://creativecommons.org/licenses/by/4.0/).

The high specific surface area and porosity of electrospun nanofibers have sparked an increasing interest in their use as ultrasensitive gas sensors [8]. Jan et al. [9] confirmed the successful entrapment of hexanal, a highly volatile molecule, in PVA nanofibers. Hexanal molecules gradually diffused through the pores. They stated that volatile hexanal can be effectively entrapped in the PVA polymer matrix, facilitating a slow diffusion process. The degree of fish spoilage increases with an increase in the number of bacteria, causing the release of more volatile amines and H_2S. Therefore, changing properties of the nanofibers could be correlated with the absorption of amines, aldehydes, or other volatiles. Recently, metal oxides have been extensively investigated and applied as sensing materials for NH_3, H_2S, DMA, TMA, and formaldehyde which are released during the spoilage of fish meat [10, 11]. SnO_2 has a lower wall thickness compared to other nanostructure types as it has a hollow nanostructure. O molecules can easily permeate and adsorb on SnO_2 because of its porous and polycrystalline structure [12]. Therefore, PVA nanofibers can be functionalized with black carrot/metal-based nanostructures to have better gas-sensing properties. In the present study, black carrot and SnO_2 functionalized nanofibers' morphological, physical, surface, and molecular properties were compared before and after storage with smoked black sea salmon fillets.

2. Material and method

2.1. Material

Polyvinyl alcohol with a molecular mass of (44,05)n g/mol was received from ZAG Industrial Chemicals. Black carrot extract powder (Doehler Chemical) (KN006298–1) and SnO_2 (Sigma Aldrich) were used for functionalizing the nanofibers. Smoked black sea salmon (*Salmo trutta labrax*) purchased from the supermarket at 4 °C with package, and was cold stored before analysis.

2.2. Method

2.2.1. Production of nanofibers and application on salmon fillets

A solution of 10 % polyvinyl alcohol dissolved in distilled water at approximately 70 °C for 30 min, prepared as the first solution (PVA). The same solution with 5 % (w/w) black carrot extract (PVAB) was prepared as the second solution and transferred to a syringe for production. Finally, for the third solution, 10 % polyvinyl alcohol, 5 % (w/w) black carrot extract, and 5 % (w/w) SnO_2 were prepared together. Electrospun nanofibers were produced under room conditions (feed rate: 0.013 mL/min; collector-syringe needle distance: 10 cm). A collector, covered with silicone-based paper, was used to collect electrospun nanofibers.

Portions of smoked salmon were placed in plastic petri dishes, and the petri dishes were sealed with stretch films. Then, nanofiber samples were placed in a semicircle shape on the films, and the petri dishes were closed with a transparent lid. It should be noted that there was no direct contact between the produced nanofibers and the black sea salmon fillets. According to the previous study [13], after the smoked salmon package was opened, the sample spoiled within 60 h and was considered unconsumable when kept at room temperature. Smoked salmon fillets were stored at room temperature for 60 h.

2.2.2. Characterization of nanofiber samples

The morphologies of the films were observed by scanning electron microscopy (SEM, Zeiss Evo® LS 10) at an accelerating voltage of 10 kV. The quantification of nanofiber diameters was determined by randomly measuring 100 nanofibers using software (ImageJ, version 1.49). The contact angle of the electrospun samples before and after storage was

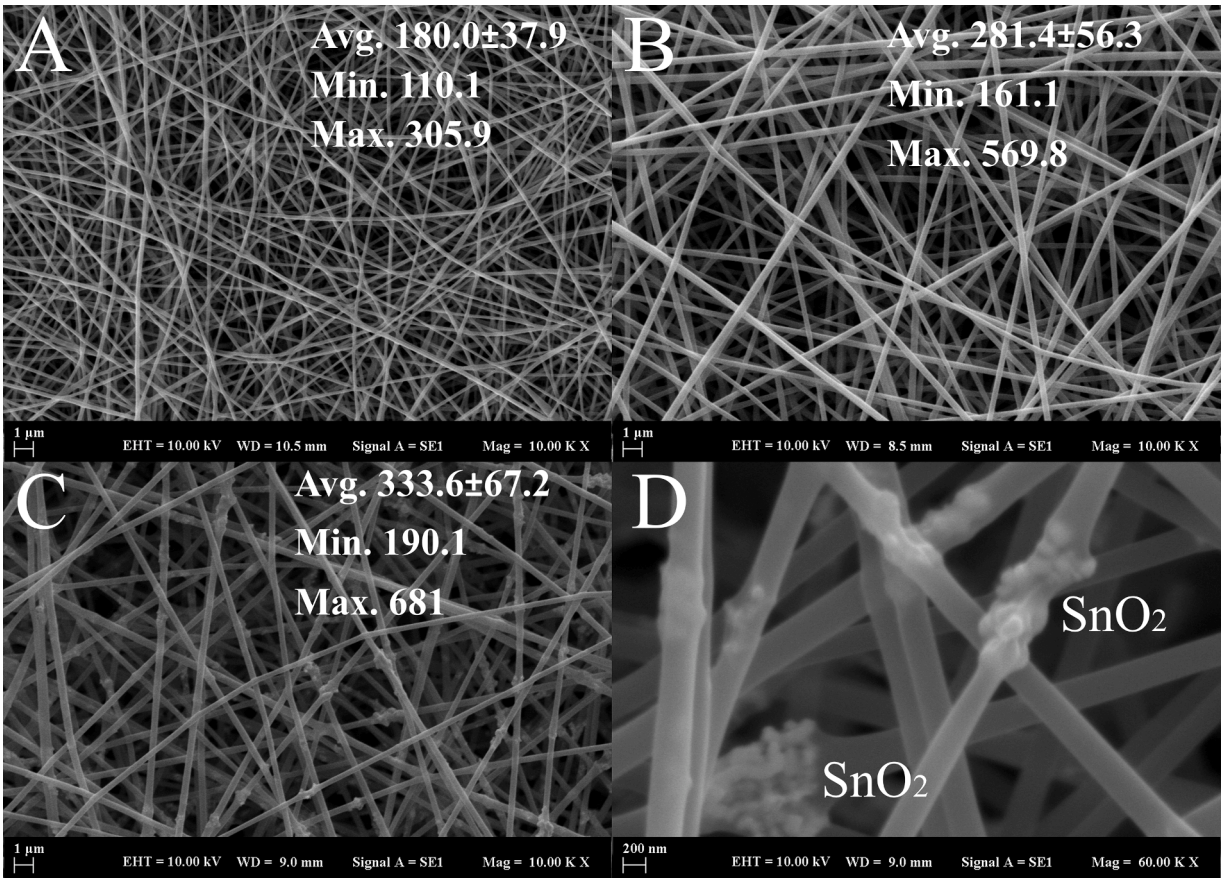


Fig. 1. Nanostructure of (A) PVA, (B) PVAB, (C) PVASN samples at 10 kX magnification and (D) PVASN at 60 kX magnification.

measured by a tensiometer. The functional groups of nanofibers were determined using Attenuated Total Reflectance-Fourier Transform Infrared (ATR-FTIR) spectroscopy device (Perkin Elmer Spectrum 100, Netherlands) by scanning in the range of 4000–650 cm^{-1}. The crystal phase of the PVASN sample before and after storage was obtained by an XRD equipment with Cu Kα radiation at 40 mA and 45 kV. The XRD pattern was scanned from 10° to 80° (2θ). The Dektak XT (Bruker) mechanical three-dimensional profilometer was used to examine the surface structure of the nanofibers before and after storage. The *L, a, b* color parameters of nanofibers before and after exposion to values were also studied by Fru® Precise Color Reader (see Supplementary Material S.1) in order to evaluate the color differences.

3. Results and discussion

3.1. Morphological characterization

As shown in Fig. 1, nanofibers formed a smooth structure without any beads or cracks. The addition of black carrot extract and black carrot-SnO_2 increased the average diameter of pure fibers from 180.0 ± 37.9 nm to 281.4 ± 56.3 nm and 333.6 ± 67.2 nm, respectively. Nanofibers without holes indicated good compatibility between polyvinyl alcohol and the extract, probably due to the hydrogen bonding between carboxyl groups (COO−) and -OH groups.

Looking closer at electrospun nanofiber samples with SnO_2 (see Fig. 1D), inhomogeneous agglomerates and clustering in some parts were observed. Newly formed structures and increased thickness of nanofibers indicate both SnO_2 integration on the surface and penetration inside the nanofibers.

Fig. 2 shows closer magnifications of the three samples with EDS results. It can be seen that the PVA sample prepared in this experiment consists of two elements: carbon (C) and oxygen (O). Carbon is the major component since polyvinyl alcohol is a vinyl polymer joined by carbon–carbon linkages [14]. After the addition of black carrot extract, oxygen showed higher intensity with a ratio of 25 % atomic weight, which is attributed to hydroxyl and carbonyl groups of anthocyanins. Many Sn peaks and a higher O peak are observed, as shown in the graph of the PVASN sample (Fig. 2C), indicating the integration of SnO_2 on the surface of nanofibers. Selected two spots showed that the aggregated part has higher Sn peaks compared to the other part, since the relative atomic ratios of Sn are determined as 11.05 % and 6.9 % for spot 1 and spot 2, respectively. Similar agglomerated bumps on surfaces based on SnO_2 are reported in previous studies [15,16]. The PVASN nanofibers presented in this work have relatively high energy gaps (3.4–3.9 eV) compared to the gaps of PVA and PVAB samples. Similarly, Matysiak et al. [15] stated that SnO_2 is a semiconductor with an energy gap of about 3.3–3.9 eV.

Elemental color analysis was applied to the PVASN sample to evaluate the distribution of main atoms (Fig. 3). Although some Sn agglomerated bumps were observed (represented by a pink color) in some parts of the image, they were generally distributed uniformly across the surface of the nanofibers. Similar results were observed in previous studies with gelatin-based nanofibers [6].

Negligible morphological changes were observed after storage with smoked salmon fillets. As shown in Fig. 4, nanofibers formed an interlaced network structures with swelling behavior. Nanofiber sizes increased to 300.3 ± 89.9 nm (PVA), 645.5 ± 173 nm (PVAB), and 603.4 ± 217.6 nm (PVASN) with the absorption of volatiles, with the

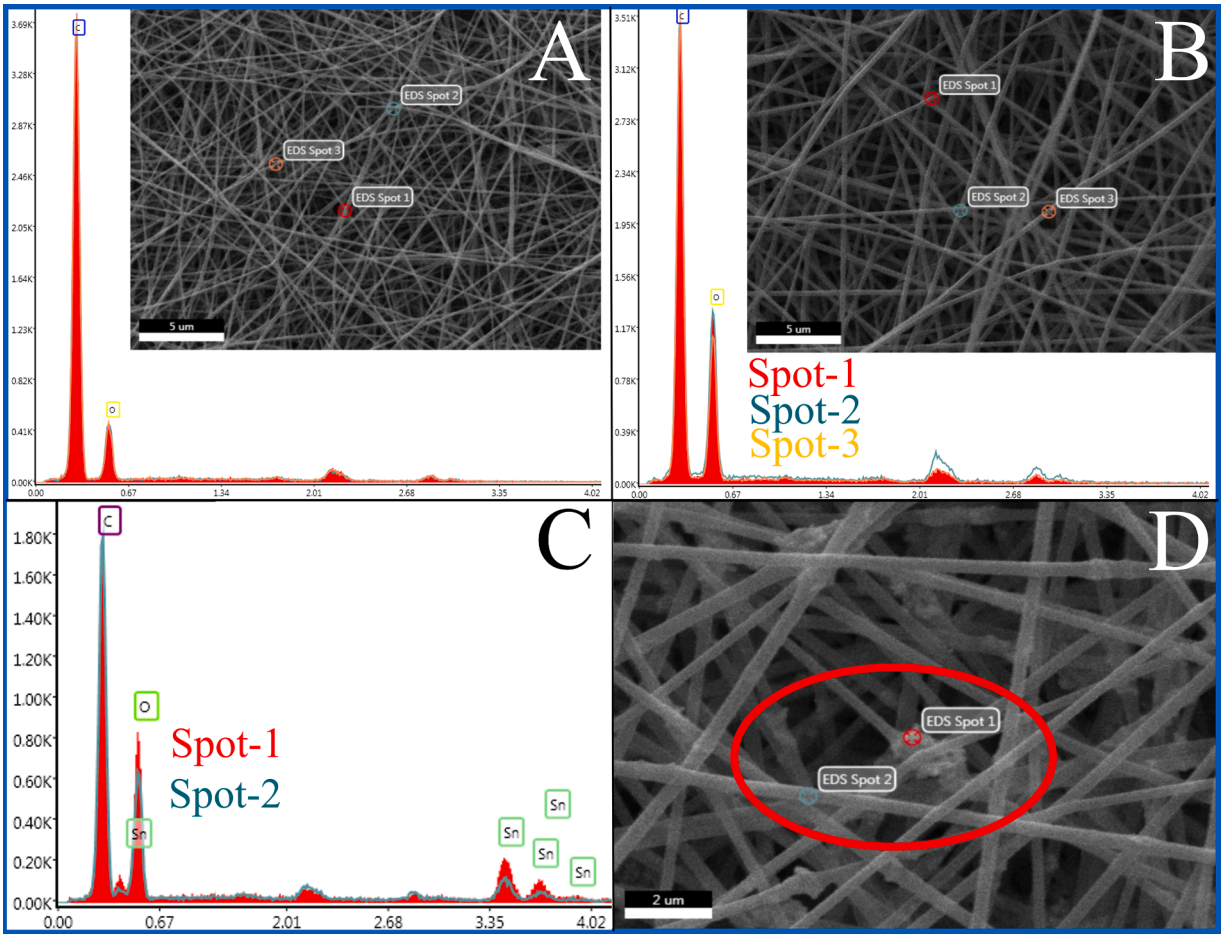


Fig. 2. SEM images (A, B, D) and EDS elemental mapping of chosen spots in (A) PVA, (B) PVAB, (C) PVASN nanofiber samples.

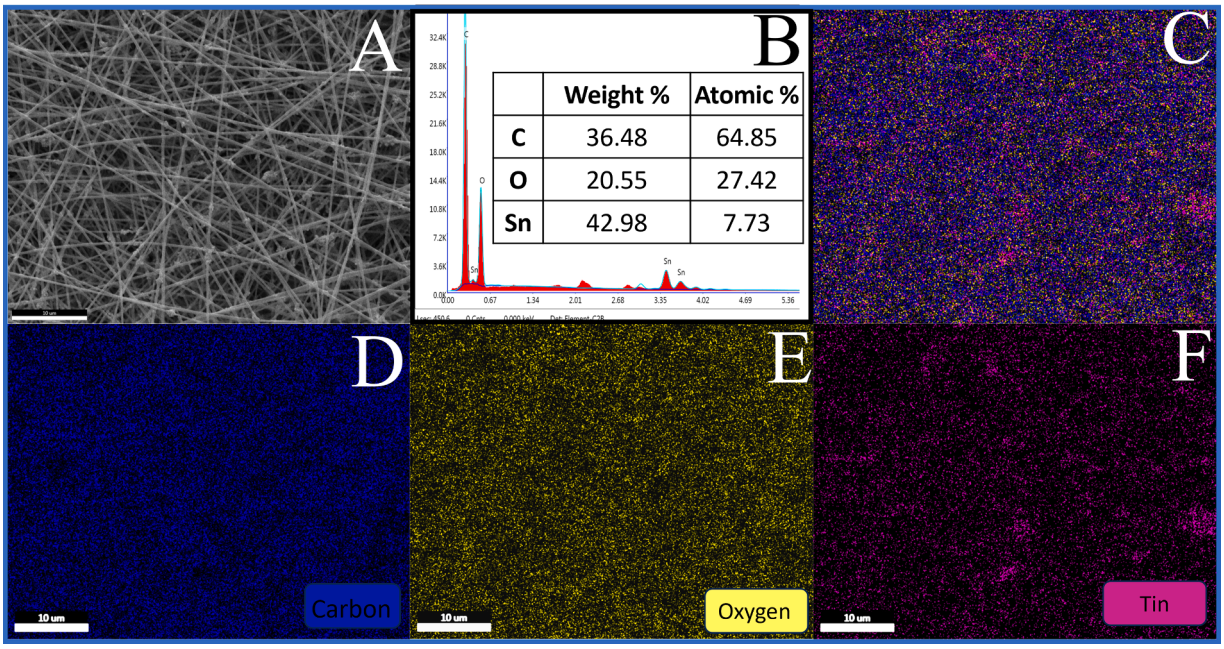


Fig. 3. PVASN nanofiber sample (A), weight and atomic percentages (B), elemental color composition atoms together (C) and seperately; Carbon (D), Oxygen (E), Tin (F).

highest change in the PVAB sample (129 %). Furthermore, inhomogeneous structures such as circle shapes, etc., were observed in the PVAB sample, probably due to interfacial H bonding with various volatile substances. Jan et al. [9] stated that polyvinyl alcohol nanofiber thickness increased from 176±32 nm to 340±100 nm after being loaded with volatile hexanal, suggesting hexanal uniformly bulges the fibers, indicating the inclusion of the matrix.

In a study by Song et al. [17] SEM images confirmed the morphology changes of the self-assembled nanofibers with the formaldehyde gas reaction. In another study [18], it was stated that opening of micro-scale pores and closure of nano-scale pores in shales due to CO_2 exposure, may lead to alteration in morphology and swelling. The volatiles gas trapping mechanism may be related to electrostatic deposition because of the opposite charges between volatiles and nanofibers, causing electrostatic attraction or chemical adsorption/desorption model [19,20]. Here when nanofibers are exposed to gasses, molecules may react with ions and release electrons into the conduction band of SnO_2. SnO_2 creates oxygen vacancies and unstable bonds on its surface which cause charge transfer with the volatiles [11,20,21]. It should be noted that PVASN sample was less intertwined and swelling behavior was lower compared to other samples. This observation may be attributed to higher stability in terms of morphology.

3.2. Water contact angle (°)

Water contact angle (WCA) of the nanofibers were measured to determine the surface wettability of samples. Water contact angle under 90° is defined as hydrophilic for structures [22]. As shown in Table 1, PVAB sample had the highest WCA with a value of 89.48 due to the presence of greater hydrophilic OH groups in anthocyanins [22].

Wettability may depend on its porosity, surface roughness, and the polymer composition of the nanofiber sample. PVASN showed lower values of WCA than PVA and PVAB, which might be attributed to the rougher surface morphologies compared to others, as it was stated that surface roughness would reduce the contact angle for a hydrophilic surface [23]. The hydrophilicity of surfaces can be enhanced by decreasing the surface roughness, and the decrease in surface roughness can improve the hydrophilicity characteristics. A hydrophobic surface can trap air, and a decrease in roughness leads to more hydrophilicity [24].

All WCA values decreased after storage, with the lowest value for PVAB. The WCA of PVASN is almost constant with a low change, suggesting that after storage, the absorption of volatiles has little effect on the hydrophilicity of the PVASN sample. It was stated that -OH and -NH_2 groups may enhance the hydrophilic property of the materials [25]. In another study, a decrement of contact angle values was attributed to amine groups [26]. Therefore, changes in wettability could be the result of a rearrangement of the polymer chains during exposure, caused by changing the state of H bonding between functional groups and water drop. Pizarro et al. [27] indicated that the transition between the Wenzel and Cassie state could be observed with the change of WCA. This effect may result from the presence of new groups oriented in different directions, interacting with the water droplets condensed on the surface [27]. WCA values may also be related to the combined effect of surface energy and roughness [28]. Upon exposure to volatile gasses from the salmon sample, absorbing new groups on the nanofiber surface may change the surface energy, which may affect hydrophilicity.

3.3. Molecular structure

The FTIR spectra of PVA nanofiber sample showed a broad peak between around 3600–3100 cm^{-1}, attributed to the stretching H bonds acting intermolecularly (see Fig. 5). The peaks at 3000–2900 cm^{-1} are attributed to the –CH_2– stretching vibration from methylene groups and asymmetric stretching CH of alkyl groups [29,30]. The bonds at 1670 cm^{-1} and 1440 cm^{-1} correspond to OH and CH_2 bendings, respectively. The peak around 1160 cm^{-1} shows C—O stretching of residual acetate groups in the PVA matrix. The bond around 820 cm^{-1} is assigned to C—C vibrations [29,30].

With the addition of black carrot extract, the band in the frequency range of 3600–3200 cm^{-1} was broadened due to the OH groups of the extract, suggesting that black carrot extract was integrated into the polyvinyl alcohol nanofibers [31]. Stronger stretching intensities between 1600 and 1000 cm^{-1} may appear with aliphatic, aromatic groups of HC, and plane deformation peaks of methyl and methylene groups that prove the presence of anthocyanins [6]. The cracks between 1050 and 1010 cm^{-1} may be attributed to the COH stretching vibration of proanthocyanins. New peaks between 1630 and 1600 cm^{-1}, belonging to

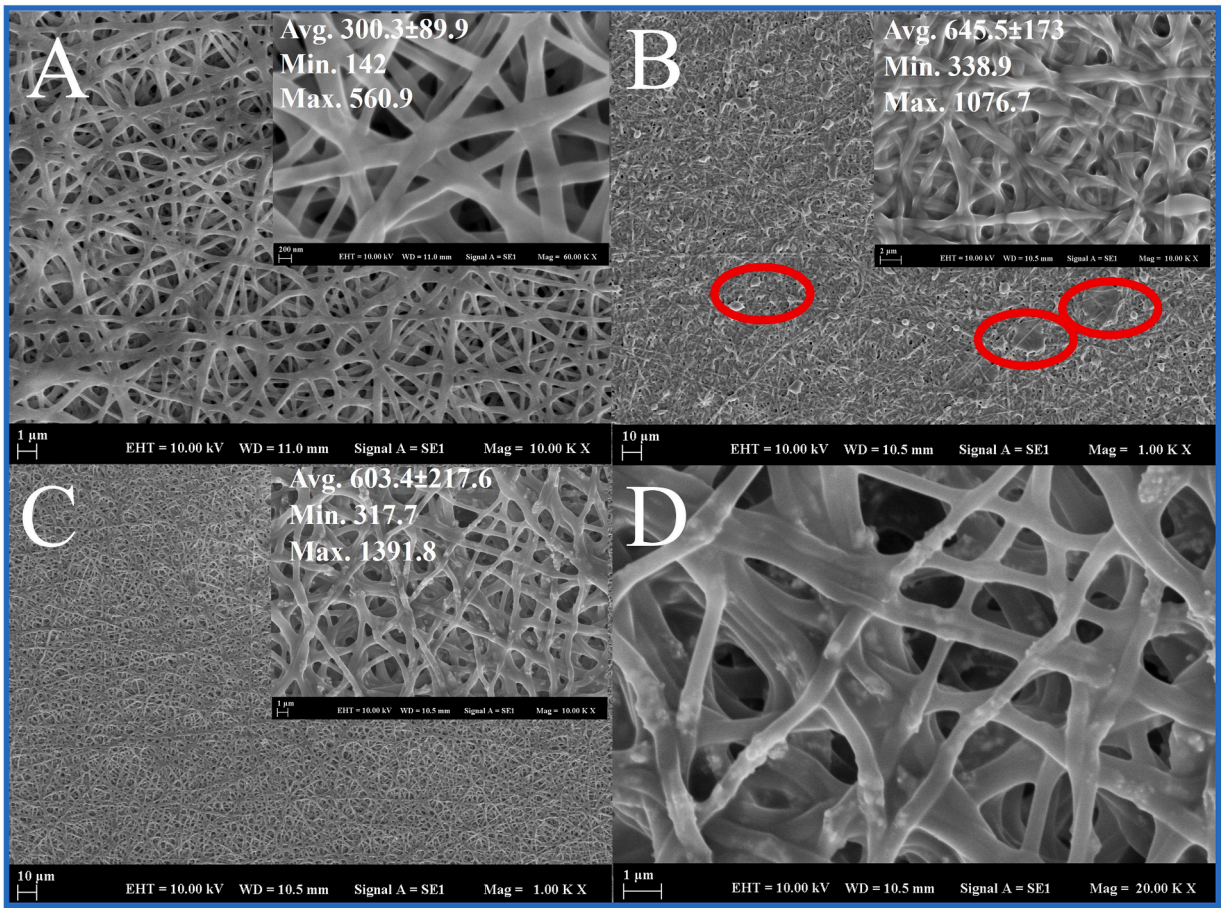


Fig. 4. SEM images of (A) PVA, (B) PVAB, (C, D) PVASN nanofiber samples after stored with salmon fillets. Inset images are magnifed views of the structures.

Table 1
Water contact angle values before and after storage.

Sample	Before Storage	After Storage
PVA	88.32±5.96	77.31±18.98
PVAB	89.48±5.96	62.93±26.78
PVASN	82.42±14.13	81.72±18.08

C = C stretching, were previously found in water extracts of black carrot samples. The shifting peak at 1700 cm^{-1} is attributed to C6 bending [32]. C—C double bonds can be recognized in the spectral wavenumber range between 1700 and 1600 cm^{-1}. Therefore, the peaks observed at 1640–1630 cm^{-1} can be ascribed to the aromatic C—C stretching in anthocyanins content. It has been stated that after immobilization of

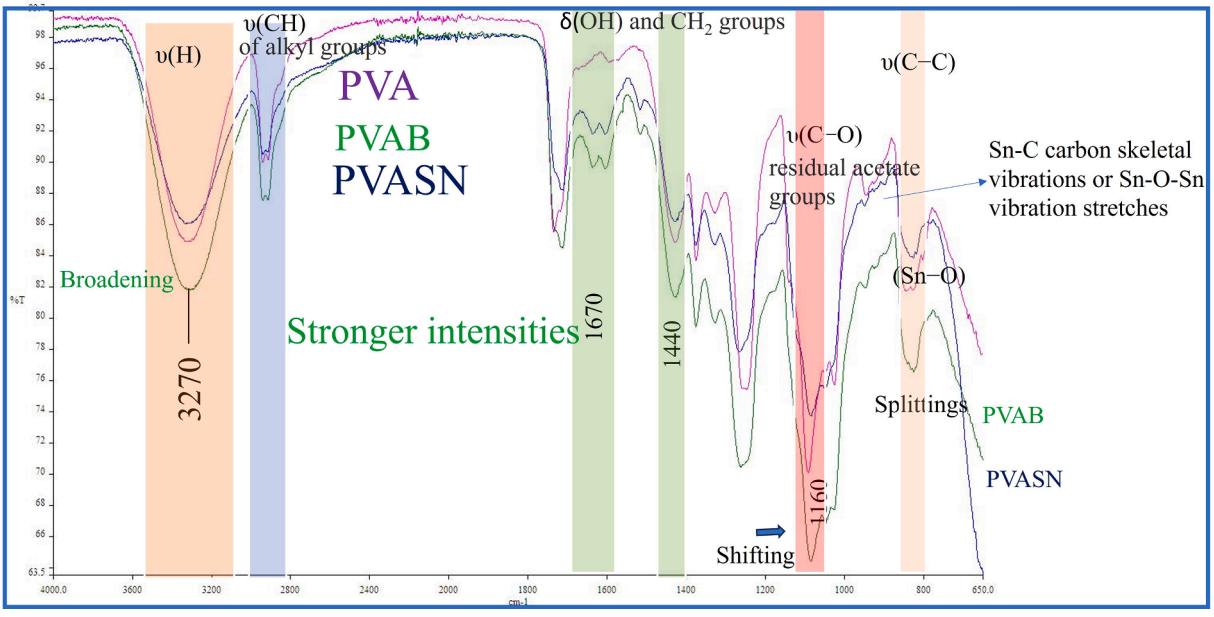


Fig. 5. The FT-IR spectrum of PVA, PVAB, PVASN nanofiber samples.

anthocyanins, a slight increase in the intensity of the band may be observed at around 1635 cm^{-1} [33].

Splittings and shiftings at approximately 1250 cm^{-1} and 850 cm^{-1} may be attributed to Sn-O bonds. New vibration peaks were observed between the 700–650 cm^{-1} region, which can be attributed to Sn-C carbon skeletal vibrations or Sn-O-Sn vibration stretches [6,32,34]. All these results reveal successful integration of SnO_2 structures.

After storage, transmittance differences were observed between 1200 and 700 cm^{-1} (Fig. 6). The reason could be attributed to the increase in the concentrations of nonprotein nitrogenous constituents and ethyl esters as a result of autolytic or microbiological proteolysis [6]. A loss of transmission is observed at 1180 cm^{-1}, and a weak shoulder near 1120 cm^{-1} is detected. This fall in transmission is ascribed to the produced free electrons upon outgassing [6,35]. Chemical cross-linking between volatiles and electrospun nanofibers caused notable differences in the spectrum after storage. Combined FT-IR spectrums are presented in Supplementary Material S.2. This result shows an interaction of the molecules in the functionalized nanofibers

3.4. XRD analysis

Crystallinity is an important material property that influences the gas sensing mechanism in SnO_2-added materials. Volatile gas molecules are likely to diffuse into nanofibers. High crystallinity may result in enhanced capabilities to interact with volatile gasses. In the current study, it was assumed that volatile gasses adsorbed on the surface of nanofibers migrate into the SnO_2 nanoparticle boundaries and then occupy the boundaries of all the agglomerated bumps. This produces electron-depleted layers at the interfaces of the two adjacent bumps, eventually building up a potential barrier for electrons to flow across, creating the gas sensing in nanofibers [36].

The XRD pattern of the initial PVASN sample exhibited a broad band between 5 and 21°, demonstrating that PVASN was in the amorphous state or has a semi-crystalline structure (see Fig. 7A). A shoulder peak was observed at 18.89°, attributed to the (101) plane of PVA semi-crystalline structures due to the occurrence of strong inter- and intra-molecular H bonding [30,37]. The Miller indices are indicated on each peak in the graph, belonging to the SnO_2 [38–40]. The peaks at 2θ ~26.65°, ~33.90°, ~38.07°, ~39.22°, ~42.69°, ~51.81°, ~57.89°, ~64.76°, ~66.02°, and ~78.76° correspond to (110), (101), (200), (111), (120), (211), (002), (112), (031), and (231) crystal planes, respectively. These peaks are indexed with the rutile or cassiterite phase of SnO_2 [11,41,42]. A similar diffractogram was observed in previous studies [16,43].

Important peaks and parameters were calculated from XRD data of PVASN nanofibers. As can be seen from the peak lists, the intensities of diffraction peaks changed after storage, indicating that the interaction with volatiles produced more irregular structures through new bonds (see Fig. 7B). Similar to the initial nanofiber, the shoulder peak was observed at 2θ = 19.5°, and d-spacing of 4.548 Å, attributed to the diffractions in plane (101) characteristic of the β-phase [44]

A stronger band around 10.2° indicates semi-crystalline diffraction [37]. It has been stated that the reduction in the crystallinity of the polymer matrix can be observed with new compounds because of disruption in ordered structures [45,46]. Decreasing peak intensities are attributed to miscibility between the crystalline and non-crystalline component [47]. Therefore, the lower crystallinity of nanofibers may be related to the absorption of volatiles released from salmon during spoilage.

There is also a shift in the 2θ position of XRD lines after exposure to released volatiles from black sea salmon (Fig. 7B). Peak shift to lower values can be caused by strain or changes in the chemical composition of nanofibers. Tensile stress is a type of stress that occurs when a material is subjected to a tensile force. This force acts to stretch or lengthen the material [48]. It has been stated that peaks in a °2θ scan can be shifted to lower angles for tensile stress, which indicates that after volatile adsorption, material stability increased against stretching [49].

Full-width at half-maximum (FWHM) measurement allowed obtaining important information about the surface state of the material [50]. Analysis of XRD peak profiles indicated that FWHM is sensitive to stress–strain accumulation in the material. An increase in stacking faults and structural disorder may widen the peaks and increase FWHM [51]. Therefore, the higher FWHM of the initial PVASN nanofiber sample before storage may be attributed to more irregular nanostructures,

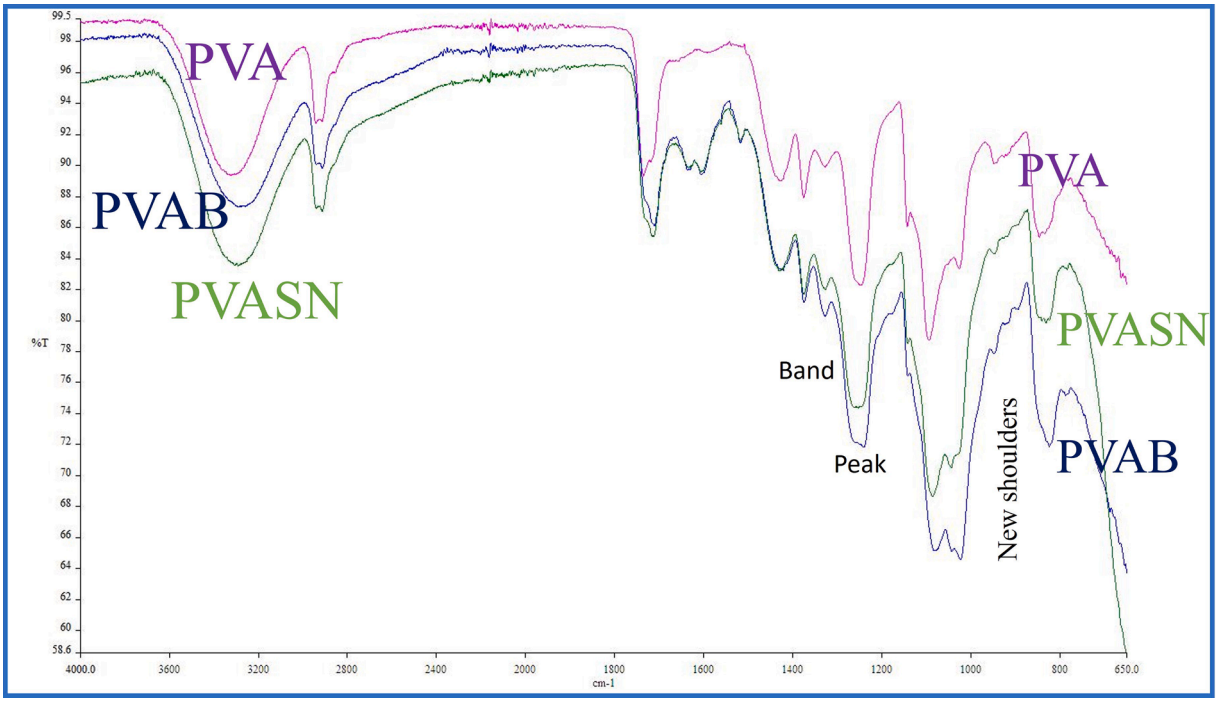
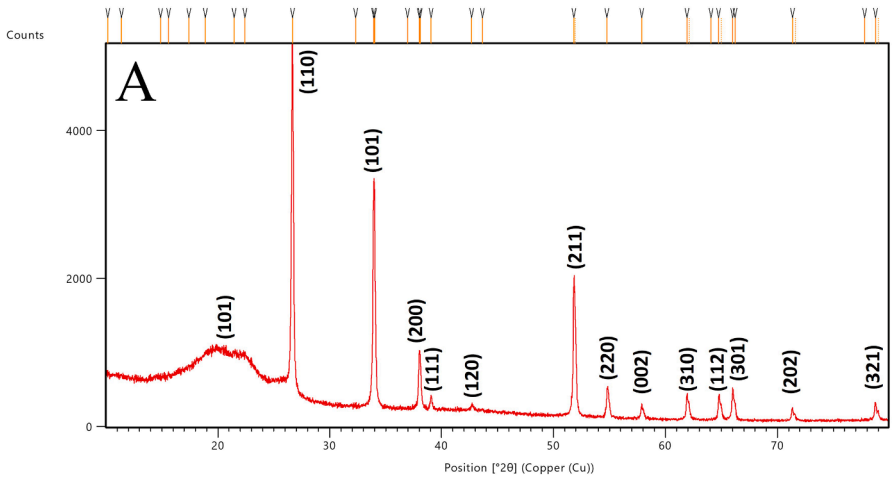
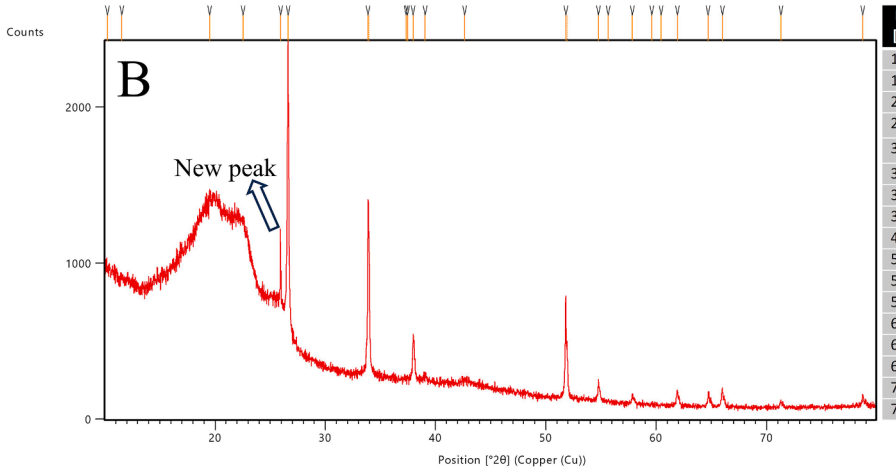


Fig. 6. The FT-IR spectrum of PVA, PVAB, PVASN nanofiber samples after stored with salmon fillets.



Pos. [°2θ]	Height [cts]	FHWM [°2θ]	d-spacing [Å]	Rel. Int. [%]
18.89	324.7	0.3070	4.695	6.91
21.46	298.8	0.2558	4.137	6.36
26.65	4696.2	0.1919	3.342	100
33.90	2790.6	0.1092	2.642	59.42
37.98	761.5	0.0936	2.367	16.22
38.07	745.3	0.0640	2.362	15.87
42.69	85.3	0.1279	2.116	1.82
51.81	1788.8	0.1560	1.763	38.09
54.78	385.7	0.0936	1.674	8.21
57.89	198.4	0.0624	1.592	4.23
61.90	325.1	0.1248	1.498	6.92
64.76	326.2	0.1560	1.438	6.95
66.02	437.7	0.0936	1.414	9.32
66.23	212.9	0.1560	1.410	4.53
71.36	147.3	0.1092	1.321	3.14
78.76	236.3	0.1092	1.215	5.03
79.01	126.1	0.1248	1.211	2.68



Pos. [°2θ]	Height [cts]	FWHM Left [°2θ]	d-spacing [Å]	Rel. Int. [%]
10.26	134.97	0.8187	8.623	7.18
19.50	200.41	0.1023	4.548	10.67
25.94	362.22	0.0768	3.433	19.28
26.61	1879.12	0.1279	3.347	100
33.89	1112.45	0.0780	2.643	59.20
33.96	830.44	0.0780	2.638	44.19
37.97	292.01	0.0624	2.368	15.54
39.04	37.75	0.3744	2.305	2.01
42.62	28.37	0.1248	2.119	1.51
51.80	652.48	0.0936	1.764	34.72
54.77	142.24	0.0936	1.675	7.57
57.84	57.16	0.0936	1.593	3.04
61.90	92.50	0.1248	1.498	4.92
64.72	94.68	0.1248	1.439	5.04
65.99	104.82	0.0936	1.415	5.58
71.31	41.72	0.1872	1.322	2.22
78.74	72.77	0.0936	1.214	3.87

Fig. 7. XRD results and peak list of PVASN sample before (A) and after (B) storage with salmon meat.

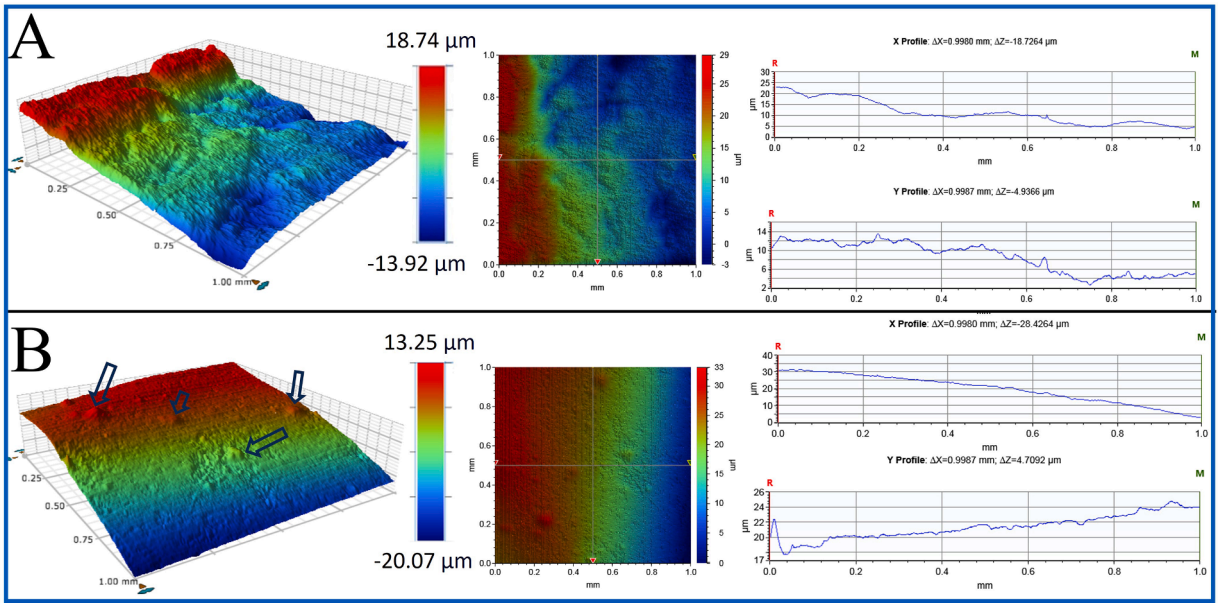


Fig. 8. 3D and 2D surface structure of PVASN nanofibers before (A) and after (B) exposed to volatiles that released from salmon fillets.

which were also confirmed by other characterization results. Furthermore, Singh et al. [52] found that FWHM decreases as the diameter of the nanotubes increases. Similarly, in the current study, after storage, the increasing diameter of nanofibers resulted in a decrease in FWHM. The hardness of the nanomaterial may also be correlated with crystallinity. An increase in hardness affects the crystallinity, which in turn causes a decrease in the FWHM of XRD peak [53]. As shown in SEM images after the absorption of volatiles, nanofiber sizes increased, which may also lead to an increase in the size of agglomerated SnO_2 particles and crystallite size. According to the Scherrer Equation, FWHM and crystallite size have a reverse relation. As the crystallite size gets bigger, FWHM decreases, and the peak gets narrower. This proves that the crystallinity of SnO_2 was changed by increasing the deposition potential, and other diffraction peaks also appeared. The presence of a new diffraction peak at $2\theta = 25.94^{\circ}$ may indicate the formation of secondary phases of tetragonal tin monoxide (SnO) with the absorption of substances [43,54].

3.5. Surface structure

Surface morphology images of PVASN sample before and after being stored with black sea salmon fillets are presented in Fig. 8A and Fig. 8B respectively. As stated in SEM results, the partial aggregation of SnO_2 nanostructure may cause an increase in the roughness of the initial nanofiber. Ranjbar et al. [24] stated that the presence of ZnO nanoparticles in the formulation of nanofibers increases the surface roughness. The formation of complexes at the border of the phases by self-organization with the presence of black carrot and SnO_2 may have caused the formation of pores in various shapes on the surface [55]. Interactions may lead to a variable and inefficient phase separation process, and therefore, a disordered structure on the surface can be observed [27].

As shown in Fig. 8A, a surface with several porous structures was obtained. However, exposing it to volatile gasses resulted in a smooth surface morphology and a fragile structure, which may be beneficial for barrier performance. Polyvinyl alcohol is a polymer that has a polar structure, and analytes have a unique molecular structure affecting its polarity [8]. Furthermore, the positions of some of the protrusions are identified (indicated by arrows). Gaussian distrubition histograms are presented in Supplementary Material S.3. Protruding may be attributed to the diffusion path for vapor when the nanofiber is exposed to volatile gas due to its adsorption capacity.

4. Conclusion

This study explores possible nanoapplications of nanofibers incorporated with black carrot extracts and SnO_2 for intelligent packaging functions in seafood products. The observed increase in average diameters of the regularly shaped nanofibers and elemental mapping results confirm the successful loading of black carrot extract and SnO_2. PVASN nanofiber sample showed higher stability compared to other samples in terms of morphological structure (PVA:66.8 %; PVAB:129 %; PVASN:81 % change in diameters) and WCA (PVA:12.4 %; PVAB:29.7 %; PVASN:0.85 % change) results. The interaction with released volatiles resulted in weaker intensity, and new shoulders and peaks were observed, suggesting that the released volatiles can affect the original structure due to the formation of complexes through new bonds. The surface structure of PVASN suggested a smoother surface morphology and a more fragile structure after storage. Differences in molecular and surface structures, and crystallinity parameters (height, FHWM, d-spacing) based on the absorption of released amine vapors during storage of nanomaterials should be further studied for intelligent food packaging functions.

Author declaration

The author declares that he has no known competing financial interests or personal relationships that could have appeared to influence the work reported in this paper.

Funding

This research did not receive any specific grant from funding agencies in the public, commercial, or not-for-profit sectors.

CRediT authorship contribution statement

Turgay Cetinkaya: Conceptualization, Formal analysis, Investigation, Methodology, Writing – original draft, Writing – review & editing.

Declaration of competing interest

The authors declare that they have no known competing financial interests or personal relationships that could have appeared to influence the work reported in this paper.

Data availability

The data that has been used is confidential.

Supplementary materials

Supplementary material associated with this article can be found, in the online version, at doi:10.1016/j.apsadv.2023.100571.

References

[1] A.A. Gürdal, T. Çetinkaya, Advancements in edible films for aquatic product preservation and packaging, Rev. Aquac. (2024), https://doi.org/10.1111/raq.12880.
[2] M. Moradi, H. Tajik, H. Almasi, M. Forough, P. Ezati, A novel pH-sensing indicator based on bacterial cellulose nanofibers and black carrot anthocyanins for monitoring fish freshness, Carbohydr. Polym. 222 (2019) 115030, https://doi.org/10.1016/J.CARBPOL.2019.115030.
[3] U. Amin, M.K.I. Khan, A.A. Maan, A. Nazir, S. Riaz, M.U. Khan, M. Sultan, P.E. S. Munekata, J.M. Lorenzo, Biodegradable active, intelligent, and smart packaging materials for food applications, Food Packag. Shelf Life 33 (2022) 100903, https://doi.org/10.1016/J.FPSL.2022.100903.
[4] O.I. Sahin, F.T. Saricaoglu, A.N. Dundar, A.F. Dagdelen, Smart applications for fish and seafood packaging systems, Green Sustain. Process Chem. Environ. Eng. Sci. (2023) 211–227, https://doi.org/10.1016/B978-0-323-95644-4.00008-5.
[5] A. Pakolpakçil, B. Osman, E.T. Özer, Y. Şahan, B. Becerir, G. Göktalay, E. Karaca, Halochromic composite nanofibrous mat for wound healing monitoring, Mater. Res. Express 6 (2020) 1250c3, https://doi.org/10.1088/2053-1591/AB5DC1.
[6] T. Çetinkaya, Zein or Gelatin Nanofibers Loaded with Au Nanospheres, SnO2 or Black Elderberry Extract Used as Active and Intelligent Packaging Layers for Various Fish Fillets, PhD Thesis, Graduate School, Istanbul Technical University, 2022.
[7] L.A. Mercante, V.P. Scagion, F.L. Migliorini, L.H.C. Mattoso, D.S. Correa, Electrospinning-based (bio)sensors for food and agricultural applications: a review, TrAC Trends Anal. Chem. 91 (2017) 91–103, https://doi.org/10.1016/J.TRAC.2017.04.004.
[8] K. Triyana, A. Rianjanu, D.B. Nugroho, A.H. As'ari, A. Kusumaatmaja, R. Roto, R. Suryana, H.S. Wasisto, A highly sensitive safrole sensor based on polyvinyl acetate (PVAc) nanofiber-coated QCM, Sci. Rep. 9 (1) (2019) 1–12, https://doi.org/10.1038/s41598-019-51851-0, 20199.
[9] N.A. Jan, K.S. Subramanian, S. Ganapathy, J. Mohanraj, K. Govindaraju, Nanofiber enabled regulated release of hexanal vapor and its impact on shelf life of mango fruits, Polymer Bull. 80 (2023) 865–881, https://doi.org/10.1007/S00289-021-04030-Z.
[10] M.V. Nikolic, Z.Z. Vasiljevic, S. Auger, J. Vidic, Metal oxide nanoparticles for safe active and intelligent food packaging, Trends Food Sci. Technol. 116 (2021) 655–668, https://doi.org/10.1016/J.TIFS.2021.08.019.
[11] B. Mahata, S. Acharyya, P. Banerji, P.K. Guha, Assessment of fish adulteration using SnO_2 nanopetal-based gas sensor and machine learning, Food Chem. 438 (2024) 138039, https://doi.org/10.1016/J.FOODCHEM.2023.138039.
[12] Z. Cai, E. Goo, S. Park, Synthesis of tin dioxide (SnO2) hollow nanospheres and its ethanol-sensing performance augmented by gold nanoparticle decoration, J. Alloys Compd. 883 (2021) 160868, https://doi.org/10.1016/J.JALLCOM.2021.160868.

[13] T. Çetinkaya, Z. Ceylan, Ambalajı Açıldıktan Sonra Buzdolabında Depolanan İki Farklı Tütsülenmiş Balık Ürününün Mikrobiyal Kalite Değişimlerinin Gözlenmesi, European J. Sci. Technol. (2019) 982–988, https://doi.org/10.31590/ejosat.649379.

[14] M. Shimao, Biodegradation of plastics, Curr. Opin. Biotechnol. 12 (2001) 242–247, https://doi.org/10.1016/S0958-1669(00)00206-8.

[15] W. Matysiak, T. Tański, W. Smok, O. Polishchuk, Synthesis of hybrid amorphous/crystalline SnO_2 1D nanostructures: investigation of morphology, structure and optical properties, Sci. Rep. 10 (1) (2020) 1–10, https://doi.org/10.1038/s41598-020-71383-2, 202010.

[16] Z. Cai, S. Park, Synthesis of Pd nanoparticle-decorated SnO2 nanowires and determination of the optimum quantity of Pd nanoparticles for highly sensitive and selective hydrogen gas sensor, Sens. Actuators B Chem. 322 (2020) 128651, https://doi.org/10.1016/J.SNB.2020.128651.

[17] J.Y. Song, S. Kim, J. Park, S.M. Park, Highly efficient, dual-functional self-assembled electrospun nanofiber filters for simultaneous pm removal and on-site eye-readable formaldehyde sensing, Adv. Fiber Mater. 5 (2023) 1088–1103, https://doi.org/10.1007/s42765-023-00279-3.

[18] D. Chandra, T. Bakshi, J. Bahadur, B. Hazra, V. Vishal, S. Kumar, D. Sen, T. N. Singh, Pore morphology in thermally-treated shales and its implication on CO2 storage applications: a gas sorption, SEM, and small-angle scattering study, Fuel 331 (2023) 125877, https://doi.org/10.1016/J.FUEL.2022.125877.

[19] H. Ji, W. Zeng, Y. Li, Gas sensing mechanisms of metal oxide semiconductors: a focus review, Nanoscale 11 (2019) 22664–22684, https://doi.org/10.1039/C9NR07699A.

[20] S. Adanur, A. Jayswal, Filtration mechanisms and manufacturing methods of face masks: an overview, J. Industrial Textiles 51 (2022) 3683S–3717S, https://doi.org/10.1177/1528083720980169.

[21] T. Senthil, S. Anandhan, Structure–property relationship of sol–gel electrospun ZnO nanofibers developed for ammonia gas sensing, J. Colloid Interface Sci. 432 (2014) 285–296, https://doi.org/10.1016/J.JCIS.2014.06.029.

[22] J. Zhang, X. Huang, J. Zhang, L. Liu, J. Shi, A. Muhammad, X. Zhai, X. Zou, J. Xiao, Z. Li, Y. Li, T. Shen, Development of nanofiber indicator with high sensitivity for pork preservation and freshness monitoring, Food Chem. 381 (2022) 132224, https://doi.org/10.1016/J.FOODCHEM.2022.132224.

[23] Y. He, S. Chen, D. Xu, D. Ren, X. Wu, Fabrication of antimicrobial colorimetric pad for meat packaging based on polyvinyl alcohol aerogel with the incorporation of anthocyanins and silver nanoparticles, Packaging Technol. Sci. 36 (2023) 745–755, https://doi.org/10.1002/PTS.2754.

[24] M. Ranjbar-Mohammadi, P. Shakoori, Z. Arab-Bafrani, Design and characterization of keratin/PVA-PLA nanofibers containing hybrids of nanofibrillated chitosan/ZnO nanoparticles, Int. J. Biol. Macromol. 187 (2021) 554–565, https://doi.org/10.1016/J.IJBIOMAC.2021.07.160.

[25] F. Wang, G. Yu, Q. Yang, X. Yi, L. Fu, Y. Wang, Antibacterial Gelidium amansii polysaccharide-based edible films containing cyclic adenosine monophosphate for bioactive packaging, Int. J. Biol. Macromol. 212 (2022) 324–336, https://doi.org/10.1016/J.IJBIOMAC.2022.05.090.

[26] A. Asiri, S. Saidin, M.H. Sani, R.H. Al-Ashwal, Epidermal and fibroblast growth factors incorporated polyvinyl alcohol electrospun nanofibers as biological dressing scaffold, Sci. Rep. 11 (1) (2021) 1–14, https://doi.org/10.1038/s41598-021-85149-x, 202111.

[27] G. del C. Pizarro, O.G. Marambio, M. Jeria-Orell, J. Sánchez, D.P. Oyarzún, R. Martin-Trasanco, F. Novio, Morphological, optical and wettability characterization of honeycomb patterned films based on self-assembling copolymer under thermal annealing, Chem. Phys. 533 (2020) 110715, https://doi.org/10.1016/J.CHEMPHYS.2020.110715.

[28] J. Zhu, Z. Liu, H. Chen, H. Liu, X. Bao, C. Li, L. Chen, L. Yu, Designing and developing biodegradable intelligent package used for monitoring spoilage seafood using aggregation-induced emission indicator, LWT 151 (2021) 112135, https://doi.org/10.1016/J.LWT.2021.112135.

[29] A. Rezaei, H. Tavanai, A. Nasirpour, Fabrication of electrospun almond gum/PVA nanofibers as a thermostable delivery system for vanillin, Int. J. Biol. Macromol. 91 (2016) 536–543, https://doi.org/10.1016/J.IJBIOMAC.2016.06.005.

[30] J.C. Ge, G. Wu, S.K. Yoon, M.S. Kim, N.J. Choi, Study on the Preparation and Lipophilic Properties of Polyvinyl Alcohol (PVA) nanofiber membranes via green electrospinning, Nanomaterials 11 (2021) 2514, https://doi.org/10.3390/NANO11102514, 2021, Vol. 11, Page 2514.

[31] A. Pakolpakçıl, Z. Draczyński, A facile design of colourimetric polyurethane nanofibrous sensor containing natural indicator dye for detecting ammonia vapour, Materials (Basel) 14 (2021) 6949, https://doi.org/10.3390/MA14226949/S1.

[32] I. Bala, S.P. Gupta, S. Kumar, H. Singh, J. De, N. Sharma, K. Kailasam, S.K. Pal, Hydrogen-bond mediated columnar liquid crystalline assemblies of C 3 -symmetric heptazine derivatives at ambient temperature, Soft Matter. 14 (2018) 6342–6352, https://doi.org/10.1039/C8SM00834E.

[33] S. Pourjavaher, H. Almasi, S. Meshkini, S. Pirsa, E. Parandi, Development of a colorimetric pH indicator based on bacterial cellulose nanofibers and red cabbage (Brassica oleraceae) extract, Carbohydr. Polym. 156 (2017) 193–201, https://doi.org/10.1016/J.CARBPOL.2016.09.027.

[34] T. Křenek, N. Murafa, P. Bezdička, J. Šubrt, H.M. Masoudi, J. Pola, IR laser-induced breakdown in tetramethyltin adjacent to Ag or Au: deposition of β-Sn nanograin-containing amorphous Au–Sn/C and Ag–Sn/C films, Appl. Organomet. Chem. 26 (2012) 135–139, https://doi.org/10.1002/AOC.2825.

[35] D. Amalric-Popescu, F. Bozon-Verduraz, Infrared studies on SnO_2 and Pd/SnO_2, Catal. Today 70 (2001) 139–154, https://doi.org/10.1016/S0920-5861(01)00414-X.

[36] S.W. Choi, J.Y. Park, S.S. Kim, Dependence of gas sensing properties in ZnO nanofibers on size and crystallinity of nanograins, J. Mater. Res. 26 (2011) 1662–1665, https://doi.org/10.1557/JMR.2011.209.

[37] S. Wu, K. Li, W. Shi, J. Cai, Preparation and performance evaluation of chitosan/polyvinylpyrrolidone/polyvinyl alcohol electrospun nanofiber membrane for heavy metal ions and organic pollutants removal, Int. J. Biol. Macromol. 210 (2022) 76–84, https://doi.org/10.1016/J.IJBIOMAC.2022.05.017.

[38] S. Khan, Zulfiqar, T. Khan, R. Khan, M. Khan, S.A. khattak, G. khan, Investigation of structural, optical, electrochemical and dielectric properties of SnO_2/GO nanocomposite, J. Mater. Sci. 30 (2019) 10202–10210, https://doi.org/10.1007/S10854-019-01356-3.

[39] B. Mondal, B. Basumatari, J. Das, C. Roychaudhury, H. Saha, N. Mukherjee, ZnO–SnO_2 based composite type gas sensor for selective hydrogen sensing, Sens. Actuators B Chem. 194 (2014) 389–396, https://doi.org/10.1016/J.SNB.2013.12.093.

[40] A. Mobasheri, S. Parhoodeh, G. Shams, Cd-doped SnO_2-reduced graphene oxide composite nanofibrous mats as CO gas sensors, Fibers Polymers 23 (2022) 784–790, https://doi.org/10.1007/S12221-022-3718-Y.

[41] Y. Zheng, J. Wang, P. Yao, Formaldehyde sensing properties of electrospun NiO-doped SnO_2 nanofibers, Sens. Actuators B Chem. 156 (2011) 723–730, https://doi.org/10.1016/J.SNB.2011.02.026.

[42] L. Sahoo, S. Bhuyan, S.N. Das, Structural, morphological, and impedance spectroscopy of Tin oxide -Titania based electronic material, Physica B Condens. Matter. 654 (2023) 414705, https://doi.org/10.1016/J.PHYSB.2023.414705.

[43] K. Daideche, H. Lahmar, D. Lerari, A. Azizi, Influence of deposition potential on the electrochemical growth and photocatalysis performance of SnO2 nanostructures, Inorg. Chem. Commun. 147 (2023) 110154, https://doi.org/10.1016/J.INOCHE.2022.110154.

[44] H. Itoh, Y. Li, K.H.K. Chan, M. Kotaki, Morphology and mechanical properties of PVA nanofibers spun by free surface electrospinning, Polymer Bulletin 73 (2016) 2761–2777, https://doi.org/10.1007/S00289-016-1620-8.

[45] J. Liu, H. Yong, Y. Liu, Y. Qin, J. Kan, J. Liu, Preparation and characterization of active and intelligent films based on fish gelatin and haskap berries (Lonicera caerulea L.) extract, Food Packag. Shelf Life 22 (2019) 100417, https://doi.org/10.1016/J.FPSL.2019.100417.

[46] X. Wang, H. Yong, L. Gao, L. Li, M. Jin, J. Liu, Preparation and characterization of antioxidant and pH-sensitive films based on chitosan and black soybean seed coat extract, Food Hydrocoll. 89 (2019) 56–66, https://doi.org/10.1016/J.FOODHYD.2018.10.019.

[47] J.J. Zhou, S.Y. Wang, S. Gunasekaran, Preparation and characterization of whey protein film incorporated with TiO_2 nanoparticles, J. Food Sci. 74 (2009) N50–N56, https://doi.org/10.1111/J.1750-3841.2009.01270.X.

[48] Difference Between Tensile Stress And Compressive Stress - Mechanical Education, (n.d.). https://www.mechanicaleducation.com/difference-between-tensile-stress-and-compressive-stress/(accessed December 24, 2023).

[49] P.S. Prevéy, X-RAY DIFFRACTION RESIDUAL STRESS TECHNIQUES, (n.d.). www.lambdatechs.com (accessed December 24, 2023).

[50] I.C. Noyan, J.B. Cohen, Residual Stress, (1987). doi:10.1007/978-1-4613-9570-6.

[51] J.M. Kim, H.T. Chung, Electrochemical characteristics of orthorhombic $LiMnO_2$ with different degrees of stacking faults, J. Power Sources 115 (2003) 125–130, https://doi.org/10.1016/S0378-7753(02)00709-7.

[52] D.K. Singh, P.K. Iyer, P.K. Giri, Diameter dependence of interwall separation and strain in multiwalled carbon nanotubes probed by X-ray diffraction and Raman scattering studies, Diam. Relat. Mater. 19 (2010) 1281–1288, https://doi.org/10.1016/J.DIAMOND.2010.06.003.

[53] H.M. Tung, J.H. Huang, D.G. Tsai, C.F. Ai, G.P. Yu, Hardness and residual stress in nanocrystalline ZrN films: effect of bias voltage and heat treatment, Mater. Sci. Eng. 500 (2009) 104–108, https://doi.org/10.1016/J.MSEA.2008.09.006.

[54] Z. Yin, M. Li, Z. Chen, X. Chen, K. Liu, D. Zhou, M. Xue, J. Ou, Y. Xie, S. Lei, C. Xie, Y. Luo, A superhydrophobic pulp/cellulose nanofiber (CNF) membrane via coating ZnO suspensions for multifunctional applications, Ind. Crops Prod. 187 (2022) 115526, https://doi.org/10.1016/J.INDCROP.2022.115526.

[55] N. Nowak, J. Tkaczewska, W. Grzebieniarz, L. Juszczak, T. Mazur, M. Szuwarzyński, P. Guzik, E. Jamróz, Active and intelligent four-layer films based on chitosan, gelatin, furcellaran and active ingredients—preparation, characterisation and application on salmon, Food Bioproc. Tech. 1 (2023) 1–14, https://doi.org/10.1007/S11947-023-03238-3.